International Forum on Aeroelasticity and Structural Dynamics
IFASD 2024
17-21 June 2024, The Hague, The Netherlands

MODELING OF SHAKER-STRUCTURE COUPLING SYSTEM AND ITS APPLICATION IN GROUND FLUTTER SIMULATION TEST

Wei Xiao[1], Changkun Yu[1], Zhigang Wu[1], Chao Yang[1,2]

[1] School of Aeronautic Science and Engineering, Beihang University, Beijing 100191, China
[2] Hangzhou International Innovation Institute, Beihang University, China

Keywords: Ground flutter simulation test, Shaker-structure coupling system, Feedforward decoupling controller

Abstract: Ground flutter simulation test (GFST) is an experimental method in the aerospace field that employs shakers to apply real-time condensed aerodynamic force to an actual structure to predict its flutter. While the controller plays an essential role in GFST, studying the mechanism of the controller can help us better design controllers. This paper proposed a modeling method of shaker-structure coupling system (SSCS)for the controllers. The proposed method is specifically suitable for linear elastic structures that follow the principle of mode superposition, and where the power amplifier of the shaker works in current mode. Ground tests of a cantilever beam and a trapezoidal elastic aluminum plate were conducted to validate the feasibility and accuracy of the method. The modeling of SSCS was utilized into the numerical simulation of GFST of the plate. And the results show that for the simple bending-torsion coupled flutter model, if the bandwidth of the controller covers the flutter frequency of the model, the controller can be used in GFST.

1 INTRODUCTION.

Ground flutter simulation test (GFST), also known as "Dry Wind Tunnel"[1], represents an innovative method to predict the flutter of structures. It loads condensed aerodynamic force calculated in specific flight conditions directly to the actual aircraft in real-time. This enables flutter predictions on the ground without wind tunnel, as shown in Figure 1.

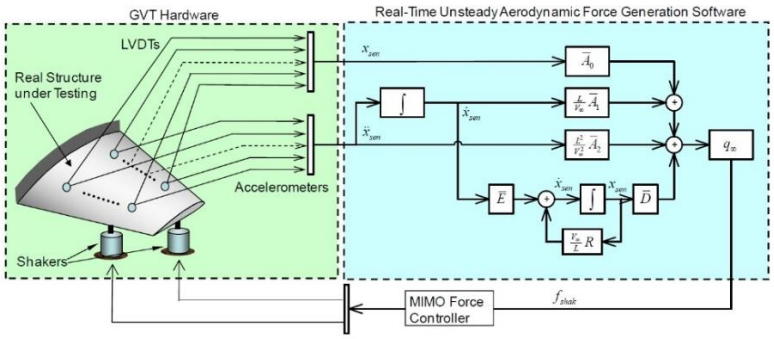

Figure 1 Diagram and blocks of GFST system[1]

While recent studies have proved the effectiveness of the method, there are still some limitations. Firstly, the complexity of real engineering objects presents great challenges in controlling multiple shakers. Secondly, the controllers also have a certain effect on the system's amplitude and phase when controlling the shakers. Different bandwidths and types of the controllers may introduce different effects to the system. All these effects may potentially influence the fluttery of the system.

Solving these challenges requires a comprehensive modeling approach for the system, and an important part of the approach is modeling of shaker-structure coupling system (SSCS). As such, this paper designed specific controllers to the system and established a comprehensive modeling of the system to analyze the effects introduced by controllers. Through this, we can enhance our understanding of the fundamentals of GFST and improve its applicability in engineering practice.

Presently, two methods are employed for this modeling: including experimental modeling and theoretical modeling. Experimental modeling involves identifying the mathematical model of the coupling system through input voltage and output actual excitation force. It is typically used in designing specific force controllers, including using transfer function models for various types of feedforward decoupling controller[2] design and employing state-space models for robust controller[4] design. Theoretical modeling simplifies the complex mechanical structure[3] and electromagnetic properties of the shaker into mathematical models. It simplifies the electrical aspect into a series circuit of resistance and inductance and simplifies the mechanical aspect into a structural dynamic model, such as a mass-spring-damping system.

In Recent years, significant contributions have been made in theoretical modeling methods for single-shaker-structure coupling system. In 1970, Tomlinson[4] established a coupling model between an electromechanical shaker and a single-degree-of-freedom structure under voltage control. In 2022, Pacini et al.[5] established a coupling model between an electromechanical shaker under voltage control and a nonlinear three-degree-of-freedom mass-spring-damping system to study the relationship between observed excitation force harmonic distortion and shaker parameters in experiments. Also in the same year, Zhang et al.[3] established a coupling model between a single shaker and a cantilever beam using Hamilton's principle. They conducted experimental validation and investigated the influence of shaker, cantilever beam parameters, and excitation point position on excitation force.

In the field of modeling for multi-shaker-structure coupling system, there have been some advancements. In 2012, Dargah et al.[6] developed a coupling model for a two-shaker-two-degree-

of-freedom system under current mode operation, deriving the transfer function between the excitation force and the Lorentz force acting on the coil. Ma et al.[7] explained the physical meaning of the parameters in the transfer function. In 2020, Mayes et al.[8] utilized the dynamic substructure approach to investigate excitation position optimization during vibration environmental tests on aircraft structures using multiple shakers. In 2022, Zhang et al.[9] applied this method to establish a coupling model for a two-shaker-cantilever beam system and conducted ground vibration test to validate the coupling model.

However, current modeling methods for multi-shaker-structure coupling systems are still in their intial stage, with the focus limited to simple control surface or plate wing models. The impact of modeling on the accuracy of ground simulation tests, in terms of amplitude and phase, remains uncertain. Moreover, this impact may become more significant with the complexity of the structure increasing, potentially leading to unexpected instabilities in the coupling system. Therefore, further research is urgently needed for more advanced modeling methods of multi-shaker-structure coupling systems.

This paper proposes a new modeling method for multi-shaker-structure coupling systems. This method is applicable to linear elastic structures that follow the principle of mode superposition, with the power amplifier of the shakers operating in current mode. The feasibility and accuracy of the modeling method were verified through ground tests on a cantilever beam and a trapezoidal elastic aluminum plate. Finally, a numerical simulation of GFST of the plate was established to introduce the application of the modeling method. Also, we explored the influence of controllers with different bandwidths to the numerical results.

2 MODELLING OF SHAKER-STRUCTURE COUPLING SYSTEM

The power amplifier of a typical electromagnetic shaker operates in both voltage mode and current mode. The output force of the shaker is more stable and less sensitive to the resonant and anti-resonant effects of the structure when the amplifier is in current mode. Therefore, this mode is more suitable for force controller design. The theoretical derivations and experiments presented in this paper were conducted with the amplifier operating in current mode. Additionally, these derivations are predicated upon two assumptions: (1) the specimen follows the principle of mode superposition as a linear elastic structure; (2) the axial stiffness of the excitation rod is sufficiently large, so that we can ignore the additional stiffness caused by the bending deformation of the exciter rod.

The internal structure of the electromagnetic shaker[10] is shown in Figure 2, consisting of a permanent magnet, a coil, a supporting spring and an excitation rod. The excitation rod is fixedly connected to the structure and a force sensor is generally used to collect the actual excitation force acting on the structure. The coil is fixed on the supporting spring, and when alternating current is applied to the coil, it generates Lorentz force to drive the coil to move axially, and then the excitation force is applied to the structure through the excitation rod.

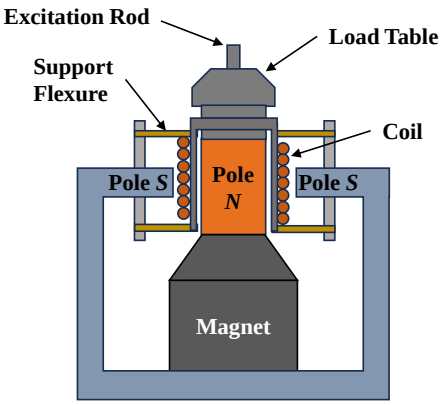

Figure 2 Internal structural of electromagnetic shaker[10]

2.1 Dynamic equation of shaker-structure coupling system

In general, the shaker is fixedly positioned either on the ground or on a platform with extremely large stiffness. It can be regarded as a single-degree-of-freedom mass-spring-damping system[11], as shown in Figure 3. Therefore, the dynamic equation of the shaker can be expressed as:

$$m_c\ddot{z}_c + c_c\dot{z}_c + k_c z_c = F_c = K_\alpha I_c \tag{1}$$

where m_c is the mass of the moving body, k_c is the stiffness of the moving body, c_c is the damping of the moving body, z_c is the axial displacement of the moving body, F_c is the Lorentz force acting on the coil, I_c is the coil current and K_α is the electromotive force constant. The Lorentz force acting on the coil is proportional to the current passing through it.

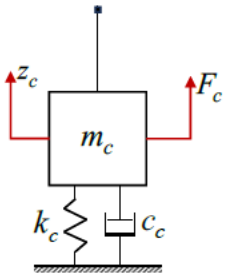

Figure 3 Mechanical model of the shaker

For shakers operating in current mode with power amplifiers, the coil resistance is significantly high. The current supplied to the shaker coil by the power amplifier varies proportionally with the input voltage[12], i.e.,

$$I_c(s) = G_\beta(s)u_c(s) \tag{2}$$

where the gain transfer function G_β approximates a first-order system and approaches a constant as frequency increases, written as K_β. Above a certain frequency, this function can be regarded as a constant, which is dependent on the electrical characteristics of the shaker. In practical applications, we found that the TIRA shaker used in this paper remains approximately constant above about 5Hz, and the MB shaker behaves similarly above about 1Hz. Therefore, above this frequency, the Lorentz force acting on the shaker coil is proportional to the input voltage of the power amplifier, i.e.,

$$F_c \approx K_\alpha K_\beta u_c \tag{3}$$

Based on this proportional relationship, when deriving the model of the SSCS, the Lorentz force can be regarded as the input external force of the coupling system, Thus, there is no need to delve deeply into the input voltage of the power amplifier, allowing the design parameters to be confined within the realm of dynamics.

Suppose there are n shakers connected to the structure at the same time. The dynamic model of the SSCS is shown in Figure 4. At the i-th excitation point, the motion displacement of the excitation point is written as z_{ei} , and the actual excitation force applied to the excitation point on the structure is written as f_{eri}. Ignoring the stiffness effect caused by the bending deformation of the excitation rod, and considering f_{eri} as the external force of the system, the structural dynamic equation can be expressed as:

$$\boldsymbol{M}_s\ddot{\boldsymbol{z}}_s + \boldsymbol{C}_s\dot{\boldsymbol{z}}_s + \boldsymbol{K}_s\boldsymbol{z}_s = \boldsymbol{f}_{er} \tag{4}$$

where $\boldsymbol{M}_s$ is the mass matrix of the structure, $\boldsymbol{C}_s$ is the damping matrix of the structure and $\boldsymbol{K}_s$ is the stiffness matrix of the structure.

In mode coordinates, according to $\boldsymbol{z}_s = \boldsymbol{\Phi}_s\boldsymbol{q}$, we can derive:

$$\boldsymbol{M}_q\ddot{\boldsymbol{q}} + \boldsymbol{C}_q\dot{\boldsymbol{q}} + \boldsymbol{K}_q\boldsymbol{q} = \boldsymbol{\Phi}_e^T\boldsymbol{f}_{er} \tag{5}$$

where $\boldsymbol{M}_q$ is the generalized mass matrix, $\boldsymbol{C}_q$ is the generalized damping matrix, $\boldsymbol{K}_q$ is the generalized stiffness matrix, $\boldsymbol{\Phi}_s$ is the mode matrix of all the structural nodes and $\boldsymbol{\Phi}_e$ is the mode matrix of excitation points. The above parameters meet the following relationship:

$$\begin{aligned}\boldsymbol{M}_q &= \boldsymbol{\Phi}_s^T\boldsymbol{M}_s\boldsymbol{\Phi}_s\\ \boldsymbol{C}_q &= \boldsymbol{\Phi}_s^T\boldsymbol{C}_q\boldsymbol{\Phi}_s\\ \boldsymbol{K}_q &= \boldsymbol{\Phi}_s^T\boldsymbol{K}_s\boldsymbol{\Phi}_s\end{aligned} \tag{6}$$

According to the force balance condition, the dynamic equation of the shaker can be expressed as:

$$\boldsymbol{m}_c\ddot{\boldsymbol{z}}_c + \boldsymbol{c}_c\dot{\boldsymbol{z}}_c + \boldsymbol{k}_c\boldsymbol{z}_c = \boldsymbol{F}_c - \boldsymbol{f}_{er} \tag{7}$$

Considering the displacement compatibility condition of the interface between the shaker and the structure, i.e.,

$$\boldsymbol{z}_c = \boldsymbol{z}_e = \boldsymbol{\Phi}_e\boldsymbol{q} \tag{8}$$

Substituting Eq.(8) into Eq.(7)

$$\boldsymbol{\Phi}_e^T\boldsymbol{m}_c\boldsymbol{\Phi}_e\ddot{\boldsymbol{q}} + \boldsymbol{\Phi}_e^T\boldsymbol{c}_c\boldsymbol{\Phi}_e\dot{\boldsymbol{q}} + \boldsymbol{\Phi}_e^T\boldsymbol{k}_c\boldsymbol{\Phi}_e\boldsymbol{q} = \boldsymbol{\Phi}_e^T\boldsymbol{F}_c - \boldsymbol{\Phi}_e^T\boldsymbol{f}_{er} \tag{9}$$

And substituting Eq.(9) into Eq.(5)

$$(\boldsymbol{M}_q + \boldsymbol{\Phi}_e^T\boldsymbol{m}_c\boldsymbol{\Phi}_e)\ddot{\boldsymbol{q}} + (\boldsymbol{C}_q + \boldsymbol{\Phi}_e^T\boldsymbol{c}_c\boldsymbol{\Phi}_e)\dot{\boldsymbol{q}} + (\boldsymbol{K}_q + \boldsymbol{\Phi}_e^T\boldsymbol{k}_c\boldsymbol{\Phi}_e)\boldsymbol{q} = \boldsymbol{\Phi}_e^T\boldsymbol{F}_c \tag{10}$$

It can be simply written as:

$$\boldsymbol{M}_c\ddot{\boldsymbol{q}} + \boldsymbol{C}_c\dot{\boldsymbol{q}} + \boldsymbol{K}_c\boldsymbol{q} = \boldsymbol{\Phi}_e^T\boldsymbol{F}_c \tag{11}$$

where $\boldsymbol{M}_c$ is the coupling mass matrix, $\boldsymbol{C}_c$ is the coupling damping matrix and $\boldsymbol{K}_c$ is the coupling stiffness matrix.

The mode frequencies of the SSCS can also be obtained by solving the generalized eigenvalue of the mass matrix and stiffness matrix, i.e.,

$$\boldsymbol{K}_c\boldsymbol{\Phi}_g = \omega_c^2\boldsymbol{M}_c\boldsymbol{\Phi}_g \tag{12}$$

where ω_c is the mode frequency of the SSCS, $\boldsymbol{q} = \boldsymbol{\Phi}_g\boldsymbol{q}_c$, $\boldsymbol{\Phi}_g$ is a mode matrix whose generalized coordinates are the mode coordinates $\boldsymbol{q}_c$ of the coupling system. Then the displacement in the physical coordinates of the system satisfies the equation:

$$\boldsymbol{z}_s = \boldsymbol{\Phi}_s\boldsymbol{q} = \boldsymbol{\Phi}_s\boldsymbol{\Phi}_g\boldsymbol{q}_c = \boldsymbol{\Phi}_c\boldsymbol{q}_c \tag{13}$$

where $\boldsymbol{\Phi}_c$ is the mode matrix of the coupling system.

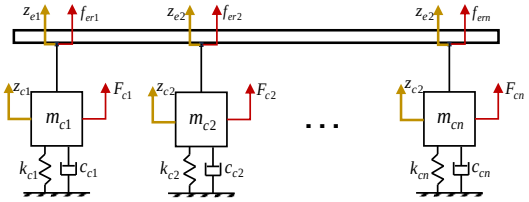

Figure 4 Mechanical model of the SSCS

2.2 Force transfer function of shaker-structure coupling system

An important purpose of modeling the SSCS is to establish the transfer function between the condensed excitation force $\boldsymbol{f}_e$, the actual excitation force $\boldsymbol{f}_{er}$ and the Lorentz force $\boldsymbol{F}_c$. Figure 5 shows the force transfer function of the coupling system and its inverse model. Once obtained, these functions can be applied in numerical simulations of GFST. This also forms the fundamental block diagram of force control methods based on the inverse model, aiming to achieve $\boldsymbol{f}_{er} \approx \boldsymbol{f}_e$.

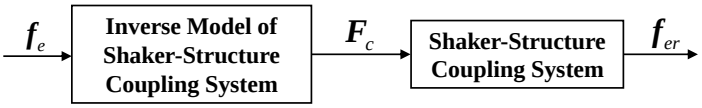

Figure 5 Block diagram of SSCS and its inverse model

From Eq.(11), it follows that:

$$\boldsymbol{q} = (\boldsymbol{M}_c s^2 + \boldsymbol{C}_c s + \boldsymbol{K}_c)^{-1}\boldsymbol{\Phi}_e^T\boldsymbol{F}_c \tag{14}$$

Substituting Eq.(14) into Eq.(7), considering the displacement compatibility condition, the force transfer function of the SSCS can be obtained:

$$\boldsymbol{f}_{er} = \left[\boldsymbol{I} - (\boldsymbol{m}_c s^2 + \boldsymbol{c}_c s + k_c)\boldsymbol{\Phi}_e(\boldsymbol{M}_c s^2 + \boldsymbol{C}_c s + \boldsymbol{K}_c)^{-1}\boldsymbol{\Phi}_e^T\right]\boldsymbol{F}_c \tag{15}$$

It can be converted into state-space equation for use in time-domain simulation of ground test. Taking the state variables as $\begin{bmatrix}\boldsymbol{q}^T & \dot{\boldsymbol{q}}^T\end{bmatrix}^T$ and the input variable as the Lorentz force $\boldsymbol{F}_c$, the state equation is:

$$\begin{bmatrix}\dot{\boldsymbol{q}} \\ \ddot{\boldsymbol{q}}\end{bmatrix} = \begin{bmatrix}\boldsymbol{0} & \boldsymbol{I} \\ -\boldsymbol{M}_c^{-1}\boldsymbol{K}_c & -\boldsymbol{M}_c^{-1}\boldsymbol{C}_c\end{bmatrix}\begin{bmatrix}\boldsymbol{q} \\ \dot{\boldsymbol{q}}\end{bmatrix} + \begin{bmatrix}\boldsymbol{0} \\ \boldsymbol{M}_c^{-1}\boldsymbol{\Phi}_e^T\end{bmatrix}\boldsymbol{F}_c \tag{16}$$

Substituting the displacement compatibility condition into Eq.(7), we can obtain:

$$\boldsymbol{f}_{er} = \boldsymbol{F}_c - \boldsymbol{m}_c \boldsymbol{\Phi}_e \ddot{\boldsymbol{q}} - \boldsymbol{c}_c \boldsymbol{\Phi}_e \dot{\boldsymbol{q}} - \boldsymbol{k}_c \boldsymbol{\Phi}_e \boldsymbol{q} \tag{17}$$

Thus, we can obtain the output equation:

$$\boldsymbol{f}_{er} = \left[-\boldsymbol{k}_c \boldsymbol{\Phi}_e + \boldsymbol{m}_c \boldsymbol{\Phi}_e \boldsymbol{M}_c^{-1} \boldsymbol{K}_c \quad -\boldsymbol{c}_c \boldsymbol{\Phi}_e + \boldsymbol{m}_c \boldsymbol{\Phi}_e \boldsymbol{M}_c^{-1} \boldsymbol{C}_c \right] \begin{bmatrix} \boldsymbol{q} \\ \dot{\boldsymbol{q}} \end{bmatrix} + (\boldsymbol{I} - \boldsymbol{m}_c \boldsymbol{\Phi}_e \boldsymbol{M}_c^{-1} \boldsymbol{\Phi}_e^T) \boldsymbol{F}_c \tag{18}$$

It's difficult to obtain the Lorentz force acting on the shaker coil in ground test. What is easier to measure is the input voltage of the power amplifier. Therefore, for comparison with experimental data, according to the proportional relationship between the Lorentz force and the input voltage of the power amplifier, as per Eq.(3), we can derive:

$$\boldsymbol{f}_{er} = \left[\boldsymbol{I} - (\boldsymbol{m}_c s^2 + \boldsymbol{c}_c s + k_c) \boldsymbol{\Phi}_e (\boldsymbol{M}_c s^2 + \boldsymbol{C}_c s + \boldsymbol{K}_c)^{-1} \boldsymbol{\Phi}_e^T \right] \boldsymbol{K}_\alpha \boldsymbol{K}_\beta \boldsymbol{u}_c \tag{19}$$

It can be simply written as:

$$\boldsymbol{f}_{er} = \boldsymbol{G}_u \boldsymbol{u}_c \tag{20}$$

2.3 Inverse model force transfer function of shaker-structure coupling system

From Eq.(5), we can obtain:

$$\boldsymbol{q} = (\boldsymbol{M}_q s^2 + \boldsymbol{C}_q s + \boldsymbol{K}_q)^{-1} \boldsymbol{\Phi}_e^T \boldsymbol{f}_{er} \tag{21}$$

The equation above indicates that if considering the actual excitation force acting on the structure as the external force, the transfer function only characterizes the dynamic properties of the structure, independent of the characteristics of the shaker. In other words, the shaker does not introduce additional effects to the structure. It should be noted that this ignores the additional mass of sensors and the additional stiffness caused by the bending deformation of the excitation rod during motion. In models whose mass and stiffness are low, these additional effects may be significant and cannot be ignored.

Substituting Eq.(21) into Eq.(7), and considering the displacement compatibility condition, we can derive:

$$\boldsymbol{F}_c = (\boldsymbol{m}_c s^2 + \boldsymbol{c}_c s + \boldsymbol{k}_c) \boldsymbol{\Phi}_e (\boldsymbol{M}_q s^2 + \boldsymbol{C}_q s + \boldsymbol{K}_q)^{-1} \boldsymbol{\Phi}_e^T \boldsymbol{f}_{er} + \boldsymbol{f}_{er} \tag{22}$$

Letting $\boldsymbol{f}_{er} = \boldsymbol{f}_e$, we can derive the force transfer function of inverse model of SSCS:

$$\boldsymbol{F}_c = [(\boldsymbol{m}_c s^2 + \boldsymbol{c}_c s + \boldsymbol{k}_c) \boldsymbol{\Phi}_e (\boldsymbol{M}_q s^2 + \boldsymbol{C}_q s + \boldsymbol{K}_q)^{-1} \boldsymbol{\Phi}_e^T + \boldsymbol{I}] \boldsymbol{f}_e \tag{23}$$

In this transfer function matrix, each parameter has its corresponding physical meaning. For such an open-loop system, due to the damping, the vibration amplitude cannot increase infinitely, hence this system is stable.

Substituting Eq.(23) into Eq.(3), we can find:

$$\boldsymbol{u}_c = \boldsymbol{K}_\beta^{-1} \boldsymbol{K}_\alpha^{-1} [(\boldsymbol{m}_c s^2 + \boldsymbol{c}_c s + \boldsymbol{k}_c) \boldsymbol{\Phi}_e (\boldsymbol{M}_q s^2 + \boldsymbol{C}_q s + \boldsymbol{K}_q)^{-1} \boldsymbol{\Phi}_e^T + \boldsymbol{I}] \boldsymbol{f}_e \tag{24}$$

It can be simply written as:

$$\boldsymbol{u}_c = \boldsymbol{G}_c^{-1} \boldsymbol{f}_e \tag{25}$$

The equation is the inverse transfer function of Eq.(20), that is $\boldsymbol{G}_c \boldsymbol{G}_c^{-1} = \boldsymbol{I}$.

3 TEST VERIFICATION

To verify the accuracy of the modeling method, this paper conducted three tests on each of the two structures, a cantilever beam and a trapezoidal plate. These tests include (1) shaker parameter identification test which can obtain the mass, stiffness and damping of the shaker's moving body; (2) mode test which can obtain the mode frequencies and mode matrix of the structure; and (3) force transfer function identification test of the SSCS which can compare the transfer function between test and numerical results.

3.1 Cantilever beam model

3.1.1 Test preparation

The test setup for the cantilever beam model is shown in Figure 6. The structure is an aluminum cantilever beam, which is 550mm long, 30mm wide and 4.8mm thick. Four PCB333B30 accelerometers, each weighing 5.0g, are arranged on the upper surface to collect vibration acceleration signals. Two TIRA shakers are used, namely TIRA S511-M (outer) and TIRA 51110-M (inner). Two KISTLER 9712B250 force sensors, each weighing 23g, are used to collect the actual excitation force. Mode test is conducted using commercial mode test system namely LMS Test-Lab. Command signal is output using NI's PXIe real-time measurement and control platform, which including a PXIe-8840 controller and a PXIe-6229 multifunction input/output devices. The experimental procedures are written by LabVIEW.

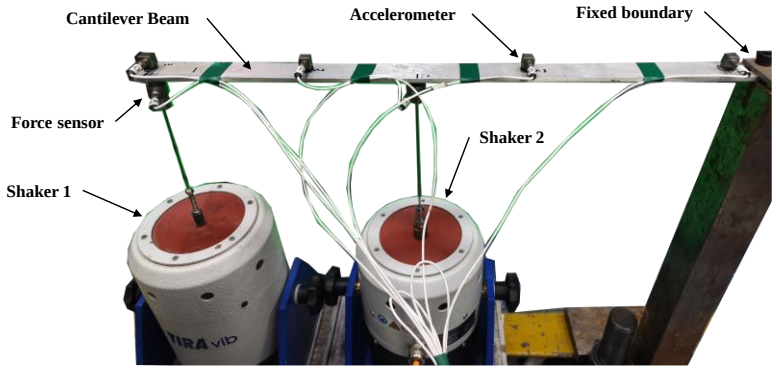

Figure 6 Test setup for the cantilever beam model

In numerical simulations, considering the influence of the additional mass of the accelerometers and force sensors on the structure, concentrated mass points are placed at the same position in the structural finite element model to simulate the sensors.

3.1.2 Shaker parameter identification test

Considering the shaker as a single-degree-of-freedom mass-spring-damping system, we hold and then release the excitation rod to allow the shaker's moving body to undergo free decay vibration. At the same time, we collect the back electromotive force from the power amplifier. From this data, we can calculate the natural frequency and damping ratio of the shaker.

At the reference state, the first-order natural frequency of the shaker is written as f_{c1}, and the damping ratio is written as ξ_{c1}. They meet the following equation:

$$f_{c1} = \frac{1}{2\pi}\sqrt{\frac{k_c}{m_c}} \tag{26}$$

When a mass block with a mass of Δm is installed on the excitation rod, then the new first-order natural frequency is written as f_{c2} and it meets the following equation:

$$f_{c2} = \frac{1}{2\pi}\sqrt{\frac{k_c}{m_c + \Delta m}} \tag{27}$$

Combining Eq.(26) and Eq.(27), the mass, the stiffness and the damping of the shaker can be calculated:

$$m_c = \frac{\Delta m}{\left(f_{c1} \diagup f_{c2}\right)^2 - 1} \tag{28}$$

The experimentally measured parameters of the shakers are listed in Table 1, and then these data will be used to establish the numerical model of the SSCS.

Table 1 Parameters of the shakers

No.	Shaker	$m_c\left(kg\right)$	$k_c\left(N/m\right)$	c_c
1	TIRA S511-M	0.153	6340.5	2.056
2	TIRA TV 51110-M	0.238	8439.8	3.048

3.1.3 Mode test

This section examines the accuracy of the coupling system by comparing the mode frequencies of first and second orders obtained from mode tests and numerical simulations. Mode tests were conducted using the hammering method on individual structure, the shaker 1-structure coupling system, the shaker 2-structure coupling system and the shakers 1/2-structure coupling system. During the tests, the power amplifiers were all enabled. To improve the accuracy of the structural model in numerical simulations, the finite element model was modified based on the mode test results of the individual structure. The comparison of the mode shapes for first and second orders is shown in Figure 7, and it demonstrates great agreement between them. It shows that the accuracy of the finite element model meets the requirements. The mode frequencies of the SSCS in numerical simulations were calculated according to the Eq.(12) . The results of the mode tests and the numerical simulations are listed in Table 2, with a maximum error is less than 1.5%. The results indicates that the proposed modeling method is feasible and can reflect the structural characteristics of the SSCS.

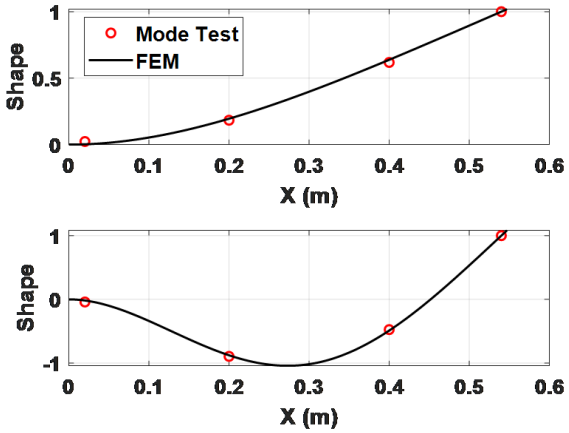

Figure 7 Mode shapes of the cantilever beam

Table 2 Mode frequencies of the shaker-structure

System	Test type	1th Frequency (Hz)	2th Frequency(Hz)
Individual structure	Mode test	10.15	62.57
	Simulation	10.20	62.81
	Error	0.5%	0.4%
Shaker 1-structure coupling system	Mode test	26.24	55.32
	Simulation	25.95	55.22
	Error	-1.1%	0.2%
Shaker 2-structure coupling system	Mode test	17.63	47.77
	Simulation	17.37	47.64
	Error	-1.5%	-0.3%
Shakers 1/2-structure coupling system	Mode test	27.25	44.34
	Simulation	26.90	43.97
	Error	-1.3%	-0.8%

3.1.4 Force transfer function identification test

The most important part of modeling the SSCS is obtaining the force transfer function of the coupling system, which is shown in Eq.(15). This transfer function can be obtained through sweep frequency tests. In these tests, the input is the voltage from the power amplifier $\boldsymbol{u}_c$ and the output is the actual excitation force $\boldsymbol{f}_{er}$. Taking two shakers as an example, the frequency response function (FRF) is identified as:

$$\begin{bmatrix} f_{er1} \\ f_{er2} \end{bmatrix} = \begin{bmatrix} \tilde{G}_{c11} & \tilde{G}_{c12} \\ \tilde{G}_{c21} & \tilde{G}_{c22} \end{bmatrix} \begin{bmatrix} u_{c1} \\ u_{c2} \end{bmatrix} \tag{29}$$

The accuracy of the coupling system modeling can be further verified by comparing the FRFs obtained through tests with numerical simulations in Eq.(20).

The test excitation signal is a 10-second burst random signal, repeated 15 times. Then the H1 estimation method was used to the averaged data to obtain the FRF. The measured gain coefficients of the power amplifiers for the two shakers are 28.4 dB and 26.7 dB. Frequency response tests were conducted for the three coupling systems, and the results were compared with numerical simulation results, as shown in Figure 8 and Figure 9. Although the test curves have some spikes in certain frequency bands due to the noise, the overall agreement between the simulation and test curves is great. This verifies that the proposed modeling method is feasible and accurate, effectively reflecting the characteristics of the SSCS. It can be used for refined numerical modeling of ground test methods.

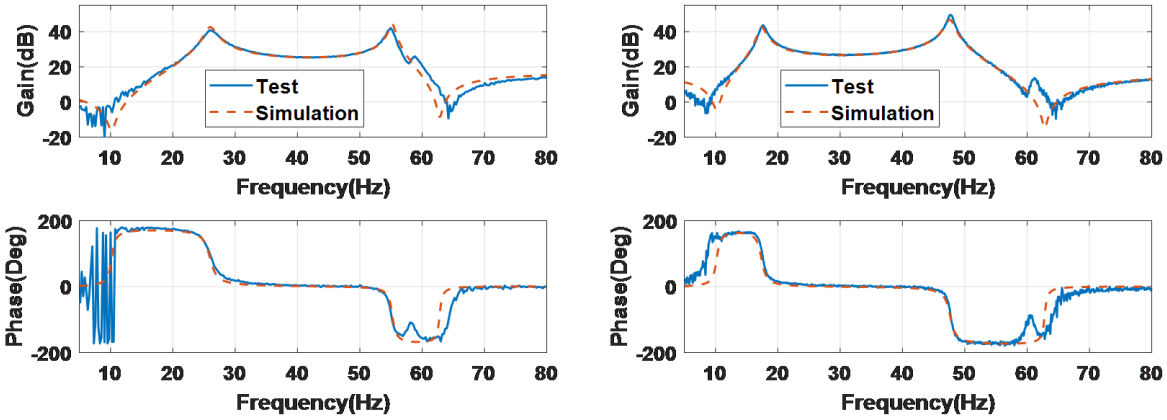

(a) Shaker 1 (b) Shaker 2

Figure 8 Force FRFs of single-shaker-structure coupling system

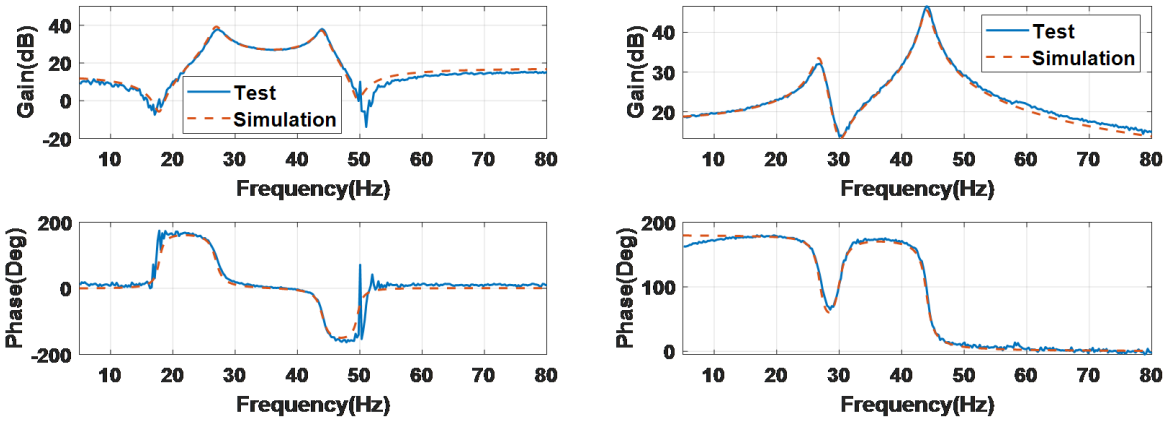

(a) G_{c11} (b) G_{c21}

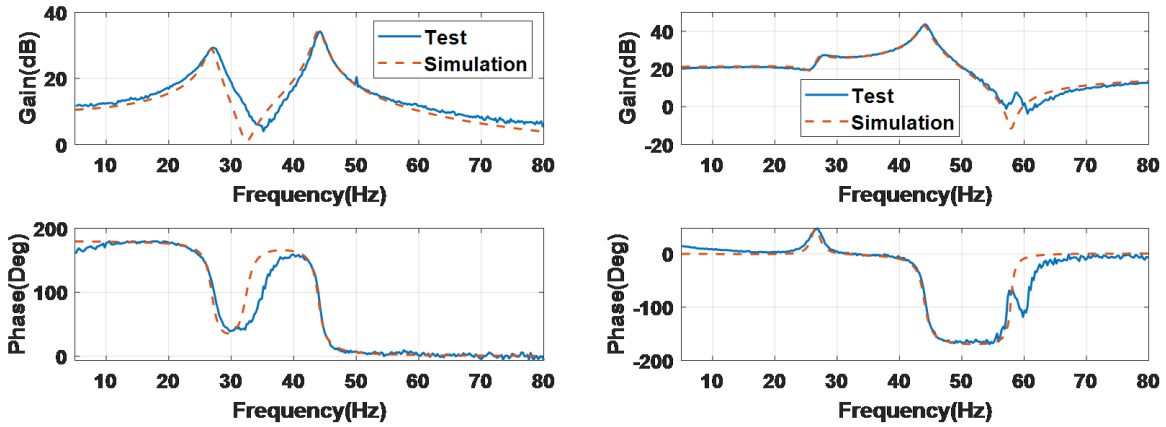

(c) G_{c12} (d) G_{c22}

Figure 9 Force FRFs of double-shaker-structure coupling system

3.2 Trapezoidal plate model

The trapezoidal plate model, made of aluminum alloy, is shown in Figure 10. The topline length of the model is 500 mm, the baseline length is 1000 mm, the height is 500 mm and the thickness is 8 mm. The test setup for the plate model is shown in Figure 11. Three shakers are used to apply the excitation force, and three force sensors are installed at the connections between the shakers and the structure to measure the excitation force. The specific models of the equipment and software used are the same as those used in the cantilever beam tests.

Firstly, shaker identification tests and mode tests were conducted. The results of the mode tests are shown in Table 3. The finite element model was modified using the mode test results to make it more accurate. Then the transfer function identification tests for the SSCS were carried out. Sweep signal was input to the three power amplifier, written as u_c, and the output excitation force is written as f_{er}. The transfer function can be derived as:

$$\begin{bmatrix} f_{er1} \\ f_{er2} \\ f_{er3} \end{bmatrix} = \begin{bmatrix} \tilde{G}_{c11} & \tilde{G}_{c21} & \tilde{G}_{c31} \\ \tilde{G}_{c12} & \tilde{G}_{c22} & \tilde{G}_{c32} \\ \tilde{G}_{c13} & \tilde{G}_{c23} & \tilde{G}_{c33} \end{bmatrix} \begin{bmatrix} u_{c1} \\ u_{c2} \\ u_{c3} \end{bmatrix} \tag{30}$$

The results of this equation are compared with the simulated results based on the Eq.(19) to better verify the accuracy of this method.

The excitation signal used in the test was a stepped sine wave signal. The signal started at 1 Hz, ended at 60 Hz, with an increment of 0.1 Hz each time. Each frequency band lasted for 1-3 seconds, with longer durations near the mode frequencies and shorter durations in other bands. The input voltage ranged from 0.1 V to 0.3 V, with lower voltages used for the outer shaker and near the mode frequencies bands, and higher voltages used in other situations. The measured gain coefficients of the three shakers were $\left[16.3\text{dB} \quad 28.2\text{dB} \quad 25.6\text{dB}\right]$. The test condition was the coupling of shakers 1/2/3 with the structure. Four sets of experimental FRFs $\tilde{G}_{c11}$、$\tilde{G}_{c22}$、$\tilde{G}_{c33}$ and $\tilde{G}_{c32}$ were compared with the simulation results, as shown in the Figure 12. In the low-frequency range, due to the characteristics of the shakers, the amplitude of the experimental FRFs is relatively

small, with a leading phase. Overall, the FRFs of the numerical simulation and the test results show great agreement. This further validates the feasibility and accuracy of the modeling method proposed in this paper, which can effectively reflect the structural characteristics of the SSCS.

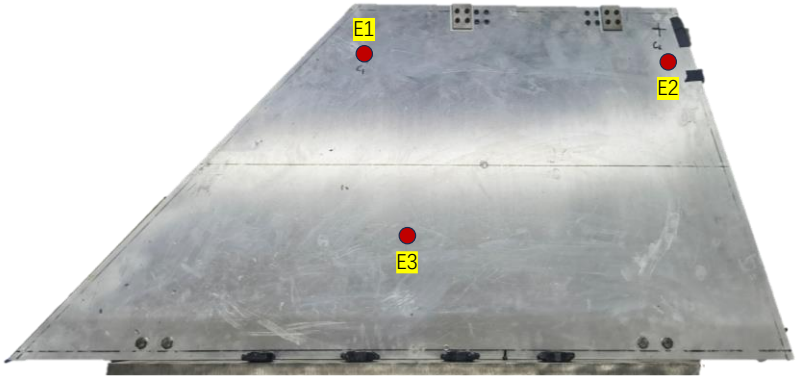

Figure 10 The picture of the plate model

Figure 11 Test setup for the plate model

Table 3 Results of the mode tests

Mode Order	Mode Frequency	Mode Damping
1	22.7	0.3%
2	58.0	0.39%

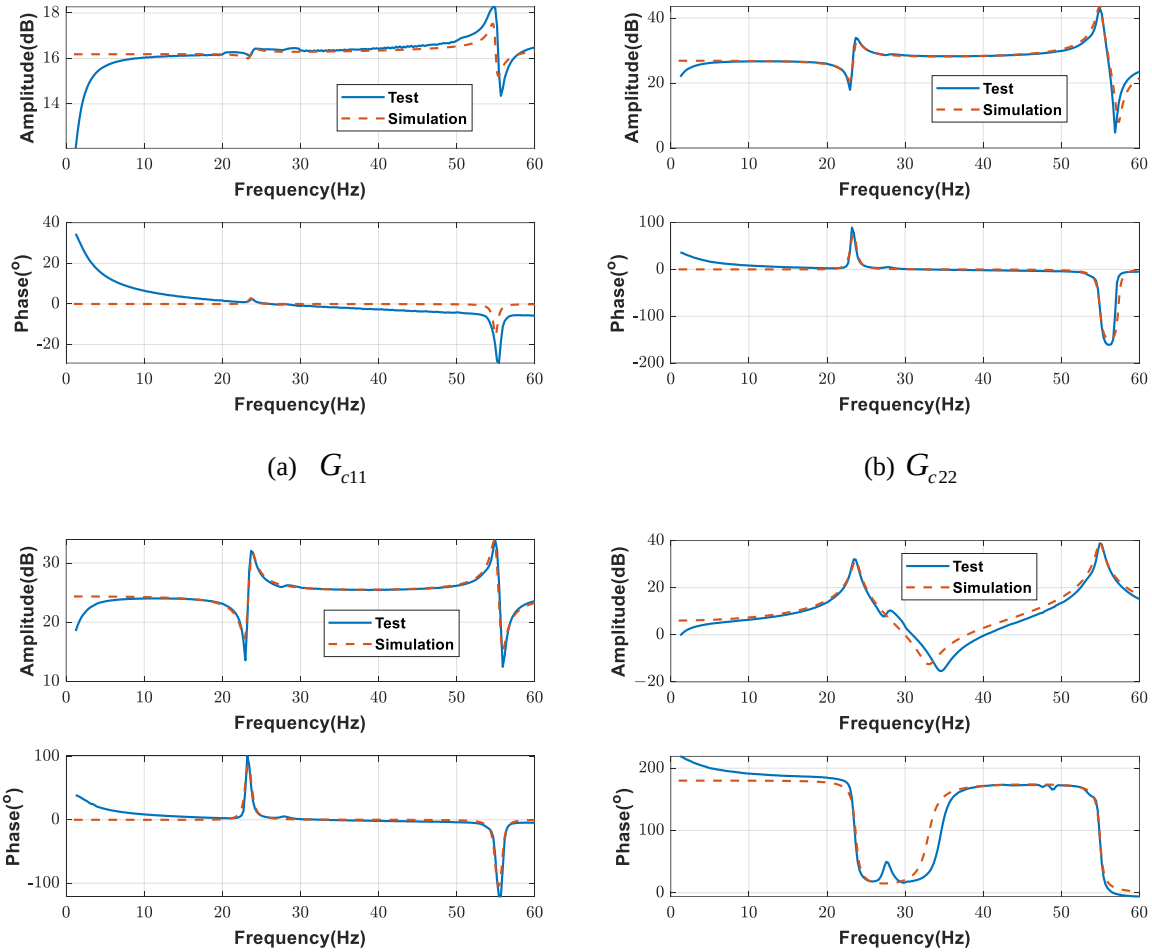

(a) G_{c11} (b) G_{c22}

(c) G_{c33} (d) G_{c32}

Figure 12 Comparison of the FRFs between test and simulation

4 NUMERICAL SIMULATION OF GFST

This paper uses a trapezoidal elastic aluminum plate as an example to introduce the application of this coupling modeling method in the numerical simulation of flutter tests. Additionally, the simulation focuses on the simple bending-torsion coupled model and investigates the influence of different bandwidths of force controllers on the test results. The program diagram of the numerical simulation of GFST is shown in Figure 13. This method takes real aircraft or components as the test object and utilizes sensors to collect vibration information of the model. Then the calculation module transfers the vibration information into the condensed excitation force under specific wind speed condition. The control module calculates the input voltages and export them to the power amplifiers to make sure the actual excitation force is nearly the same as the condensed excitation force. Subsequently, the shakers output the actual excitation force to the model, and the model deforms again under the actual excitation force, elastic force and inertial force. Thus, these form a closed-loop. This can test whether the structure is stable at that wind speed and obtains the aerodynamic elastic stability of the structure under different conditions by changing the condensed excitation force calculation conditions.

In our numerical simulations, the method of the solver is Runge-Kutta and the step size of calculation is 0.0001 second. The total time of the numerical simulation is 2 seconds. The time-domain signal of the z-direction response at measurement point 1 is taken as the observation target. White noise is added as a disturbance signal when outputting the condensed aerodynamic forces.

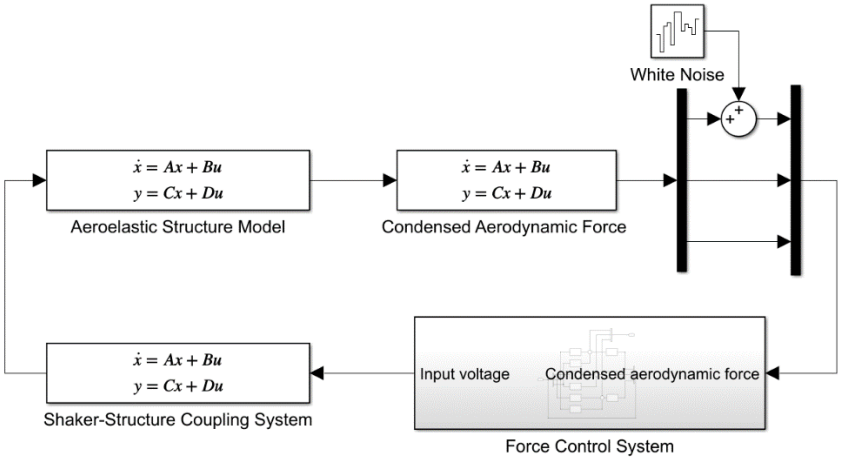

Figure 13 Block diagram of the numerical simulation of GFST

4.1 Condensed aerodynamic force

The aerodynamic model of the structure is shown in Figure 14, and the condensed aerodynamic force frequency-domain equation at the excitation points is obtained using the dipole grid method[1]:

$$\boldsymbol{f}_e = q_\infty \boldsymbol{G}_e^T \boldsymbol{S}\boldsymbol{A}(\boldsymbol{G}_m' + i\frac{k}{b}\boldsymbol{G}_m)\boldsymbol{z}_m \tag{31}$$

where q_∞ is the dynamic pressure, $\boldsymbol{G}_e$ is the interpolation matrix from the excitation points to the pressure centroids of the aerodynamic grids, $\boldsymbol{S}$ is the aera of the aerodynamic grids, $\boldsymbol{A}$ is the matrix of aerodynamic force coefficients, $\boldsymbol{G}_m$ is the interpolation matrix of measurement points to control points on the aerodynamic grids, $\boldsymbol{G}_m'$ is the interpolation matrix of partial derivatives in the streamwise direction from measurement points to interpolation points, $k = \dfrac{\omega b}{V}$ is the reduced frequency, ω is the circular frequency of harmonic vibration, b is the reference length, V is the flight velocity and $\boldsymbol{z}_m$ is the displacement of the measurement points.

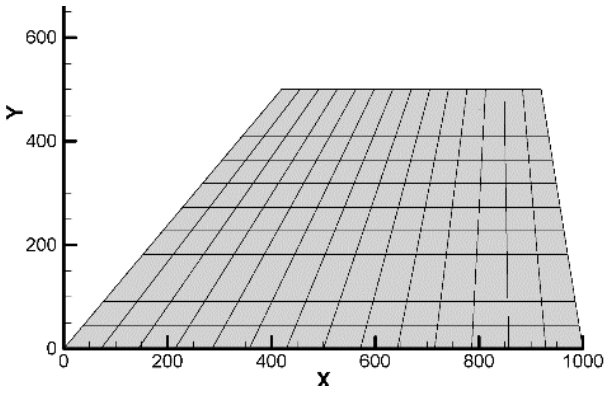

Figure 14 Aerodynamic model of the plate model

Since it's inconvenient to calculate the frequency-domain equation in real-time, it needs to be converted into time-domain form. This can be achieved through minimun-state rational function fitting:

$$\boldsymbol{f}_e = q_\infty(\boldsymbol{A}_0 + \frac{b}{V}\boldsymbol{A}_1 s + \frac{b^2}{V^2}\boldsymbol{A}_2 s^2)\boldsymbol{z}_m + q_\infty \boldsymbol{D}(\boldsymbol{I}s - \frac{V}{b}\boldsymbol{R})^{-1}\boldsymbol{E}s\boldsymbol{z}_m \tag{32}$$

where $\boldsymbol{A}_0, \boldsymbol{A}_1, \boldsymbol{A}_2, \boldsymbol{D}, \boldsymbol{E}, \boldsymbol{R}$ all are coefficient matrices in the fitting process.

In order to facilitate calculation and use, it is converted into state space equation:

$$\begin{cases} \dot{\boldsymbol{z}}_p = \left[\frac{V}{b}\boldsymbol{R}\right]\boldsymbol{z}_p + \begin{bmatrix}\boldsymbol{0} & \boldsymbol{E} & \boldsymbol{0}\end{bmatrix}\begin{bmatrix}\boldsymbol{z}_m \\ \dot{\boldsymbol{z}}_m \\ \ddot{\boldsymbol{z}}_m\end{bmatrix} \\ \boldsymbol{f}_e = \left[q_\infty \boldsymbol{D}\right]\boldsymbol{z}_p + \begin{bmatrix} q_\infty \boldsymbol{A}_0 & q_\infty \frac{b}{V}\boldsymbol{A}_1 & q_\infty \frac{b^2}{V^2}\boldsymbol{A}_2 \end{bmatrix}\begin{bmatrix}\boldsymbol{z}_m \\ \dot{\boldsymbol{z}}_m \\ \ddot{\boldsymbol{z}}_m\end{bmatrix} \end{cases} \tag{33}$$

where $\boldsymbol{z}_p = (\mathrm{s}\,\boldsymbol{I} - \frac{v}{b}\boldsymbol{R})^{-1}\boldsymbol{E}s\boldsymbol{z}_m$.

4.2 Optimization of the measurement points and excitation points

When calculating the condensed aerodynamic force, it is assumed that the generalized aerodynamic force calculated through interpolation is equal to the original structural generalized aerodynamic force. In other words, the mode shapes of the points interpolated from the measurement points and the excitation points on the aerodynamic grids are consistent with their own mode shapes[13]. Therefore, when selecting measurement points and excitation points, it is necessary to satisfy this condition. In this paper, using the error between the interpolated mode shapes and the original mode shapes as the objective function when selecting points, genetic algorithms are employed to select suitable measurement points and excitation points on the structure. Finally, the optimized positions of the points are shown in Figure 15.

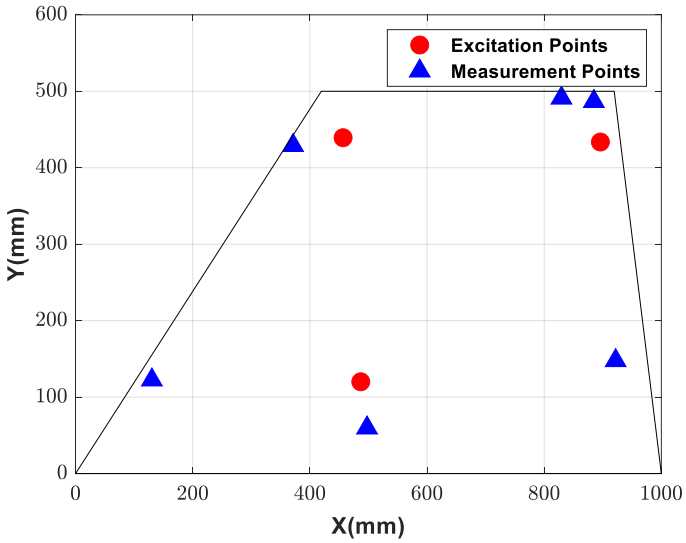

Figure 15 The positions of excitation points and measurement points

4.3 Force control system

After determining the measurement points and excitation points, the transfer function between the input voltage and the actual excitation force can be established by combining the shaker parameters from Table 1, the finite element model parameters of the structure, and Eq.(19). The gain of the power amplifier $K_\alpha K_\beta$ varies each time it is used, so it is set to 1 during numerical simulation. Due to the coupling between the shakers and the structure, the excitation force calculated by Eq.(33) cannot be directly to the structure as expected. Therefore, a controller needs to be designed to control the shaker output force to ensure that the actual excitation force is consistent with the condensed aerodynamic force. When designing the controller, since the actual excitation force applied to the structure satisfies the principle of linear superposition, the transfer function from the input voltage of each channel to the actual excitation force of all three channels can be obtained through single-channel frequency sweep excitation. This process is repeated three times to obtain the transfer function from the input voltage of all channels to the actual excitation force of all channels. Subsequently, the feedforward decoupling controller can be designed as [14]:

$$\begin{bmatrix} u_{c1} \\ u_{c2} \\ u_{c3} \end{bmatrix} = \begin{bmatrix} \tilde{G}_{c11}^{-1} & 0 & 0 \\ 0 & \tilde{G}_{c22}^{-1} & 0 \\ 0 & 0 & \tilde{G}_{c33}^{-1} \end{bmatrix} \left(\begin{bmatrix} f_{e1} \\ f_{e2} \\ f_{e3} \end{bmatrix} - \begin{bmatrix} 0 & \tilde{G}_{c12} & \tilde{G}_{c13} \\ \tilde{G}_{c21} & 0 & \tilde{G}_{c23} \\ \tilde{G}_{c31} & \tilde{G}_{c32} & 0 \end{bmatrix} \begin{bmatrix} u_{c1} \\ u_{c2} \\ u_{c3} \end{bmatrix} \right) \tag{34}$$

4.4 Aeroelastic structure system

In numerical simulation, it is also necessary to calculate the structural response of the measurement points when subjected to the excitation forces at the excitation points. The generalized structural dynamics equation for the measurement points under the application of actual excitation forces is:

$$\boldsymbol{\Phi}_m^T \boldsymbol{M}_s \boldsymbol{\Phi}_m \ddot{\boldsymbol{q}}_m + \boldsymbol{\Phi}_m^T \boldsymbol{C}_s \boldsymbol{\Phi}_m \dot{\boldsymbol{q}}_m + \boldsymbol{\Phi}_m^T \boldsymbol{K}_s \boldsymbol{\Phi}_m \boldsymbol{q}_m = \boldsymbol{\Phi}_e^T \boldsymbol{f}_{er} \tag{35}$$

where $\boldsymbol{\Phi}_m$ is the mode matrix of the measurement points and $\boldsymbol{q}_m$ is the generalized displacement of the measurement points.

It can also be written as the state space equation:

$$\begin{cases} \begin{bmatrix} \dot{\boldsymbol{q}}_m \\ \ddot{\boldsymbol{q}}_m \end{bmatrix} = \begin{bmatrix} \boldsymbol{0} & \boldsymbol{I} \\ -\boldsymbol{M}_s^{-1}\boldsymbol{K}_s & -\boldsymbol{M}_s^{-1}\boldsymbol{C}_s \end{bmatrix} \begin{bmatrix} \boldsymbol{q}_m \\ \dot{\boldsymbol{q}}_m \end{bmatrix} + \begin{bmatrix} \boldsymbol{0} \\ \boldsymbol{M}_s^{-1}\boldsymbol{\Phi}_e^T \end{bmatrix} \boldsymbol{f}_{er} \\ \begin{bmatrix} \boldsymbol{z}_m \\ \dot{\boldsymbol{z}}_m \\ \ddot{\boldsymbol{z}}_m \end{bmatrix} = \begin{bmatrix} \boldsymbol{\Phi}_m & \boldsymbol{0} \\ \boldsymbol{0} & \boldsymbol{\Phi}_m \\ -\boldsymbol{\Phi}_m\boldsymbol{M}_s^{-1}\boldsymbol{K}_s & -\boldsymbol{\Phi}_m\boldsymbol{M}_s^{-1}\boldsymbol{C}_s \end{bmatrix} \begin{bmatrix} \boldsymbol{q}_m \\ \dot{\boldsymbol{q}}_m \end{bmatrix} + \begin{bmatrix} \boldsymbol{0} \\ \boldsymbol{0} \\ \boldsymbol{\Phi}_m\boldsymbol{M}_s^{-1}\boldsymbol{\Phi}_e^T \end{bmatrix} \boldsymbol{f}_{er} \end{cases} \tag{36}$$

4.5 Influence of force controller bandwidth

Based on the above theory, a numerical simulation of GFST for the trapezoidal elastic aluminum plate can be established. When the observation signal remains constant at a certain amplitude and frequency for harmonic vibration, as shown in the Figure 16 (a), indicating that the plate will flutter under this speed. The flutter frequency can be obtained by applying Fourier transformation to the data, as shown in Figure 16 (b).

Giving sweep signal to the coupling system, and we can get the output from the numerical simulation. Through these data, the transfer function of the coupling system can be obtained. For convenience of use, it is necessary to fit this transfer function to obtain its mathematical model. When fitting the transfer function, the fitting bandwidth can have a significant impact on the control effect. This paper investigates the impact of controller designed based on transfer function obtained from fitting with different bandwidths on the test results.

When designing the first controller, considering that the flutter of the model is caused by the coupling of the first and the second order modes, the bandwidth of the controller is set to 10-60 Hz. Taking G21 as an example, the curve “Fitted Result 1” shown in the Figure 17 is fitted with this bandwidth. After using the controller, taking the control effect of the channel 2 as an example, the transfer function from the condensed excitation force to the actual excitation force is shown in Figure 18. It can be found that in most of the bandwidth form 10-60 Hz, the magnitude-frequency curve remains stable around 1, and the phase-frequency curve remains stable near 0 degree. Near the first and second order mode frequencies of the model, the curve has some fluctuations, but the fluctuation of the magnitude-frequency curve is generally within 20%, and the fluctuation of the phase-frequency curve is generally within 5 degrees. It can be considered that the controller designed under this condition can achieve satisfactory control effects for the condensed excitation force with in the 10-60 Hz bandwidth.

When designing the second controller, considering that the flutter frequency is around 40 Hz, the bandwidth of the controller is set to 35-45 Hz, as shown by curve “Fitted Result 2” in Figure 17. After using the controller, taking the control effect of the channel 2 as an example, the transfer function from the condensed excitation force to the actual excitation force is shown in Figure 18. Outside the bandwidth of 35-45 Hz, the magnitude-frequency curve generally fluctuates by more than 20%, with some even exceeding 200%, and the phase-frequency curve fluctuates up to 120 degrees, thinking it uncontrollable. Within the bandwidth of 35-45Hz, the control effect is consistent with the previous controller. It can be considered that this controller has significant control effect within the 35-45 Hz, but it is ineffective outside this bandwidth.

The comparison between two sets of numerical simulations results using different controllers and theoretical flutter results is shown in Table 4. It can be concluded that for the simple bending-

torsion coupled flutter model, when the controllers using the decoupling method based on the transfer function and inverse transfer function satisfy the following conditions: (1) the controller is stable, and (2) the bandwidth of the controller includes the flutter frequency of the model, the designed controller can be applied to GFST of the model with high accuracy. In the test conducted by Wu[13], the bandwidth of the controller is 26-36 Hz, only including the bandwidth around the flutter frequency but not the mode frequencies. The test results are consistent with the theoretical results, thus proving the conclusion the influence of controller bandwidth proposed in this paper.

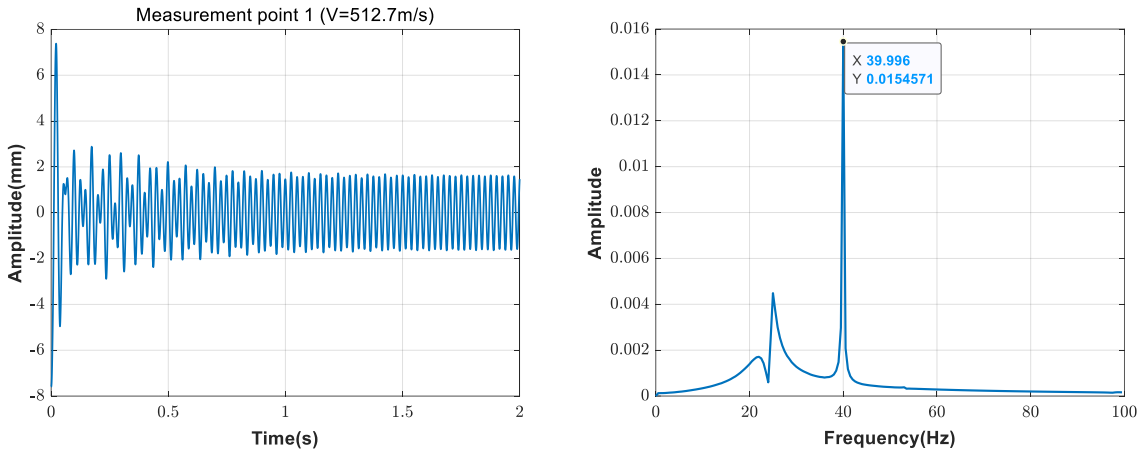

(a) The time-domain signal of the z-direction response (b) The flutter frequency of the model

Figure 16 Numerical simulation results

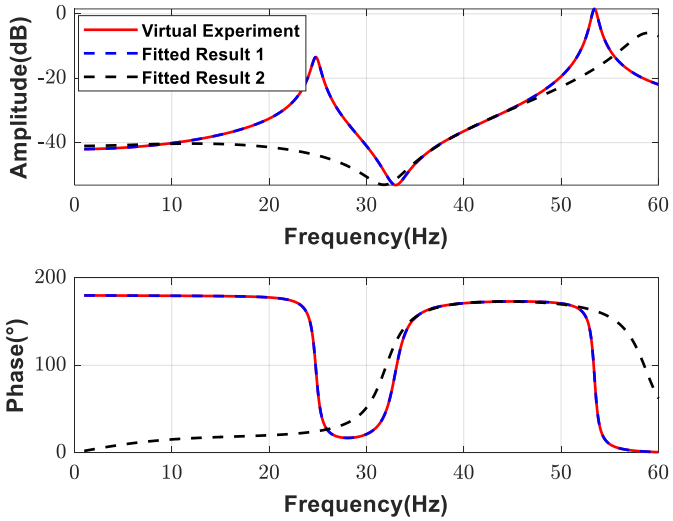

Figure 17 Comparison of the FRFs of the virtual experiment and fitted results

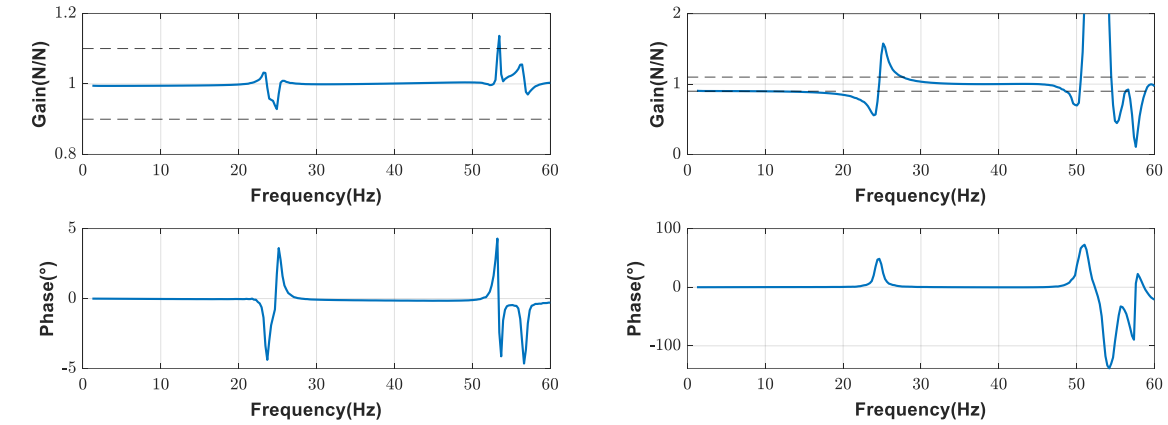

(a) Control effect of controller 1 (b) Control effect of controller 2

Figure 18 Two FRFs between the condensed excitation force and the actual excitation force

Table 4 Different results of the flutter tests

Test Condition	Flutter Velocity	Flutter Frequency
Theoretical Results	516.7m/s	40.1Hz
Controller 1	512.7m/s	40.0Hz
Controller 2	515.8m/s	40.0Hz

5 CONCLUSION

1) This paper proposes a modeling method for the SSCS. And this method is applicable to linear elastic structures that satisfy the principle of mode superposition, with the shaker power amplifier operating in current mode. Furthermore, the feasibility and accuracy of this method are validated through ground tests of FRFs for a cantilever beam and a trapezoidal elastic aluminum plate.
2) The numerical simulation of the plate shows that for the simple bending-torsion coupled flutter model, the feedforward decoupling controllers can be applied to GFST of the model if them satisfy the following conditions: (1) the controllers are stable, and (2) the bandwidth of the controllers covers the flutter frequency of the model.

This modeling method can also be applied to refined modeling in other numerical simulation of ground aeroelastic stability simulation tests. Through this, research can be conducted on force controller design methods, shaker-structure coupling interference, system time delay, and other aspects, which facilitating the engineering application of GFST.

REFERENCE

[1] Zeng J., Kingsbury D., Ritz E., Chen P.C., Lee D.H., Mignolet M., GVT-based ground flutter test without wind tunnel. *52nd AIAA/ASME/ASCE/AHS/ASC Structures, Structural Dynamics and Materials Conference*, 2011, 1942.

[2] Yun J.M., Han J.H., Development of ground vibration test based flutter emulation technique. *Aeronaut j*, 2020, 124(1279), 1436-1461.

[3] Zhang G., Wang X., Yang Z., Study on excitation force characteristics in a coupled shaker-structure system considering structure modes coupling. *Chinese Journal of Aeronautics*, 2022, 35(7), 227-245.

[4] Tomlinson G.R., Force distortion in resonance testing of structures with electro-dynamic vibration Exciters. *Journal of Sound and Vibration*, 1979, 63(3), 337-350.

[5] Pacini B.R., Kuether R.J., Roettgen D.R., Shaker-structure interaction modeling and analysis for nonlinear force appropriation testing. *Mechanical Systems and Signal Processing*, 2022, 162.

[6] Hassan Pour Dargah M., Effects of shaker impedance and transducer cross-axis sensitivity in frequency response function estimation. *University of Cincinnati*, 2012.

[7] Ma C., Wu Z., Yang C. Determination of the dynamic characteristics of a multi-point excitation system using electrodynamic shakers and control of their exciting force. *Journal of Vibration Engineering and Technologies*, 2016, 4(2), 161-173.

[8] Mayes R., Ankers L., Daborn P., Moulder T., Ind P., Optimization of shaker locations for multiple shaker environmental testing. *Experimental Techniques*, 2020, 44(3), 283-297.

[9] Zhang G., Li W., Wang X., Yang Z., Influence of flexible structure vibration on the excitation forces delivered by multiple electrodynamic shakers. *Mechanical Systems and Signal Processing*, 2022, 169.

[10] Lang G.F., Electrodynamic shaker fundamentals. *S V Sound and Vibration*, 1997, 31(4), 14-23.

[11] Rao D.K., On the glitches in the force transmitted by an electrodynamic exciter to a structure. *58th Shock and Vibration Symposium, NASA, Scientific and Technical Information Branch*, 1987, 245-255.

[12] Varoto P.S., Oliveira L.P.R., On the force drop off phenomenon in shaker testing in experimental modal analysis. *Shock and Vibration*, 2002, 9(4-5), 165-175.

[13] Wu Z., Ma C., Yang C., New approach to the ground flutter simulation test. *Journal of Aircraft.* 2016, 53(5), 1578-1580.

[14] Yu C., Wu Z., Yang C., Real-time ground aeroservoelastic test for slender vehicles based on condensed aerodynamic force loading. *Aerospace.* 2024, 11(2), 105.

COPYRIGHT STATEMENT